International Journal of Heat and Technology
Vol. 43, No. 2, April, 2025, pp. 479-492
Journal homepage: http://iieta.org/journals/ijht

Numerical Analysis of Burner Position and EFB-Coal Co-Firing Effects on Combustion Performance and Emissions in Pulverized Coal Boilers

I Nyoman Agus Adi Saputra[1], Prabowo[1*], Atok Setiyawan[1], I Gusti Bagus Wijaya Kusuma[2], Sobar Ishan[1], Arif Darmawan[3], Hariana[3]

[1] Department of Mechanical Engineering, Institut Teknologi Sepuluh Nopember (ITS), Surabaya 60111, Indonesia
[2] Department of Mechanical Engineering, Universitas Udayana, Bali 80361, Indonesia
[3] Center for Energy Conversion and Conservation, National Research and Innovation Agency (BRIN), Jakarta 10340, Indonesia

Corresponding Author Email: prabowo@me.its.ac.id

https://doi.org/10.18280/ijht.430210

Received: 14 February 2025
Revised: 1 April 2025
Accepted: 16 April 2025
Available online: 30 April 2025

Keywords:
co-firing, empty fruit bunches, computational fluid dynamic (CFD), low-rank coal, pulverized, boiler

ABSTRACT

The co-firing of renewable biomass fuels, such as oil palm empty fruit bunches (EFB), with low-rank coal (LRC) in pulverized coal boilers, has emerged as a promising strategy for reducing carbon emissions while utilizing agricultural waste. This study investigates the effects of burner injection position and fuel composition on combustion performance through comprehensive computational fluid dynamics (CFD) simulations of a 315 MWe pulverized coal boiler. The research focuses on comparing EFB injection between the lower (Burner A) and upper (Burner D) burner zones at co-firing ratios of 5%, 15%, and 25% on a thermal basis. Numerical simulations were conducted using Reynolds-Averaged Navier-Stokes (RANS) equations, along with species transport and discrete phase models. Key parameters analyzed include temperature distribution, CO_2 mass fraction, and NOx/SO_2 emissions. The results demonstrate that EFB injection at Burner D generates significantly higher temperature increases (54.82 K at 5% EFB and 85.36 K at 25% EFB) compared to Burner A (9.74 K at 5% EFB and 34.10 K at 25% EFB). Emission analysis indicates that all co-firing scenarios result in reduced CO_2 and NOx emissions compared to pure coal combustion, with maximum reductions occurring at a 25% EFB loading. Notably, the configuration of Burner A demonstrates superior emission reduction performance, even though it achieves lower temperature gains. The study concludes that the injection from the upper burner (D) enhances combustion efficiency, while the positioning of the lower burner (A) offers better emission control. A 25% EFB co-firing ratio is identified as optimal for balancing temperature maintenance and emission reduction. These findings provide critical insights for optimizing biomass co-firing configurations in coal-fired power plants.

1. INTRODUCTION

Global warming is one of the most pressing environmental issues facing the world today, primarily due to the concentration of greenhouse gases, particularly carbon dioxide (CO_2) [1]. The concentration of CO_2 in the atmosphere has surged significantly in the era of global industrialization, accounting for approximately 76% of total greenhouse gas (GHG) emissions [1, 2]. This situation is primarily attributed to the increasing reliance on electric power in energy consumption, predominantly derived from the extensive use of fossil fuels (coal, natural gas, and oil), which collectively produce around 30 billion tons of CO_2 emissions annually [3]. It is imperative to reduce these emissions to mitigate climate change and limit the global temperature increase below 2℃ [4].

Electricity is a crucial driver of the rapid development of the global economy, powering industries, developing technology, and improving living standards worldwide. According to BP Energy Company's statistical review, coal-fired thermal power plants generated 35.1% of the world's electricity in 2020 [1]. Coal power will continue to play a vital role in ensuring global energy and electricity security for the foreseeable future. Despite the abundance of global coal reserves, concerns about energy depletion have increased in recent years [2-4]. This situation has increased interest in utilizing low-rank coal (LRC), particularly lignite [5]. Lignite offers several advantages over high-rank coal, such as lower mining costs, high volatility, and fewer pollution-causing impurities [6]. However, its inherent drawbacks, including high moisture content, lower heating value, and reduced power generation efficiency, significantly limit its widespread use in power generation [3].

Biomass fuels are recognized as a sustainable and valuable energy source with the potential to reduce carbon emissions, nitrogen oxides, and other pollutants [5]. However, biomass production remains limited, and the technology for combustion and transportation is still underdeveloped [6, 7]. Consequently, the large-scale use of biomass is primarily in the exploratory phase. Despite this, co-firing technology for biomass is advancing in several regions, and its application is becoming increasingly widespread. This approach offers a promising solution to address many pollution issues in the energy sector by integrating biomass with coal in power plant boilers [8, 9].

To date, the sector capable of sustainably providing large quantities of biomass for Indonesia is the waste generated from oil palm plantations, supported by the extensive area of managed land area [10, 11]. Recent statistics indicate that approximately 15.34 million hectares are dedicated to this purpose, with an estimated production of 56.49 million tons of crude palm oil (CPO) this year [12]. Given this vast land and production capacity, there is significant potential to optimize the country's renewable energy (EBT) targets, particularly in the electricity generation sector [13-15]. One of the products generated that is feasible for co-firing is an empty fruit bunch (EFB) [16]. Despite challenges such as a high moisture content ranging from 60-70%, which can hinder combustion quality in power generation systems, EFB remains a promising option due to its status as the most abundant waste produced during oil palm fruit harvesting, accounting for 21-23% per tonne [16-18]. Pretreatment methods such as heat treatment, hydrothermal processing, and torrefaction can potentially reduce EFB moisture content and improve its viability as biomass fuel [19].

Studies on the utilization of biomass as a co-firing fuel have been extensively conducted through both numerical simulations and experimental approaches. These studies explore the feasibility and benefits of integrating biomass with fossil-based fuels in energy conversion processes. Hariana et al. [20] investigated the use of EFB and palm fronds as a co-firing mixture with lignite coal in Dual Fuel Systems (DTFs). They found that the optimal mixture condition was 25% biomass; however, this mixture presented an increased risk of slag formation and material deposition, as well as a decrease in the melting temperature of the ashes. Taha et al. [21] confirmed that co-firing coal and biomass can lead to ash deposition sticking to the wall areas. Aziz et al. [22] simulated the co-firing of other palm oil waste (palm kernel shell) and found that the combustion characteristics and emissions, such as CO_2, CO, and SOx, were optimal at a mixture of 25%.

Meanwhile, Jiang et al. [23] conducted numerical simulations on torrefied EFB in a tangential boiler to increase calorific value and decrease moisture content. Their findings indicate that co-firing can reduce NOx and SOx emissions while enhancing combustion characteristics in the furnace. However, efficiency may be compromised when the co-firing mixture exceeds 50%. In addition, Li et al. [24] explored the feasibility of biomass torrefaction through simulations of combustion characteristics, devolatilization, and kinetic parameters. Their research suggests that biomass torrefaction can be a viable option for replacing coal using co-firing technology.

In contrast to previous studies, Darmawan et al. [25] treated EFB using hydrothermal methods and simulated the process with a Drop Tube Furnace (DTF) to analyze temperature distribution, heat behavior, and combustion gases. Their findings indicate that HT-EFB performs optimally in co-firing scenarios with mass fractions ranging from 10% to 25%. Ghenai et al. [26] discovered that NOx and CO_2 emissions can be reduced by co-firing coal and biomass, depending on the type of mixture and material properties involved. Generally, higher mixture ratios lead to more significant reductions in emissions. However, Rahman [27] reported that the increasing temperatures during the co-firing of various palm wastes in front-rear type boilers could increase NOx emissions. To date, the application of biomass co-firing in the power generation industry ranges from 5-10% [28]. An essential concern in biomass co-firing relates to the emission quality standards set by the regulatory authorities, which establish maximum limits applicable to plants using biomass PM: 300 mg/Nm³ SO_2: 600 mg/Nm³ NO_x: 800 mg/Nm³ [29]. In comparison, the European Union enforces stricter emission limits for biomass power plants, e.g., 50 mg/Nm³ for PM and 200 mg/Nm³ for NO_x [30]. On the other hand, Japan and South Korea implemented a regulatory incentive system for biomass co-firing, with customized emission limits based on the proportion of the fuel mixture [31].

Based on the previously mentioned studies, biomass combustion with coal has emerged as a transitional solution [4-6]. However, current research primarily focuses on fuel blending ratios [7-9] and pretreatment methods [10-12]. Notably, there have been no investigations into the impact of co-injecting cassava in different burner zones --specifically, the lower burner zone (LBZ) at the primary air inlet (Burner A), compared to the upper burner zone (UBZ) at the primary air inlet (Burner D). This oversight leaves a critical gap in understanding how the position of burner injection affects combustion performance. Therefore, this study aims to conduct a customized 3D simulation. The research will examine substitution levels of co-firing from 5%-25% and will compare the combustion temperatures in the furnace, as well as CO_2, SO_2, and NOx emissions in the PC boiler. Ultimately, this research aims to determine the most suitable approach for EFB co-firing.

2. METHODS

2.1 Domain pulverized coal (PC) boiler

PC boiler design represents an existing coal-fired power plant with a capacity of 315 Mwe. The overall height of the boiler, as constructed at the plant, is 63,700 mm, while the height from the Hopper Zone is 57,700 mm. It features a rectangular horizontal cross-section with a width of 13,700 mm and a depth of 14,700 mm [32, 33]. The furnace height, measured from the base of the hopper zone to the base of the Panel Division superheater plate, is 40,500 mm; this area is also known as the furnace exit gas temperature (FEGT) zone.

Initially, the system was equipped with five groups of primary air nozzles (A-E); however, only four groups (A-D) are actively used during operation, with one group (PA E) kept in reserve. Seven groups of secondary air nozzles (#AA, #AB, #BC, #CD, #DD, #DE, #EF) and one group of CCOFA nozzles (CCOFA-EFF) are positioned between heights of 24,140 mm and 24,500 mm at the corners of the boiler, as illustrated in Figure 1. During combustion, PC and air injected from the burners at each corner create a rotating fireball that ascends toward the center of the furnace with details of the materials used in Table 1. The boiler's combustion zone is divided into three sections: The hopper zone at the bottom, the combustion zone where fuel and air are introduced, and the upper zone for combustion gases. This combustion zone extends from the end of the hopper zone to the furnace nose. Primary and secondary air nozzles are strategically placed in lower and upper groups, defining the LBZ, UBZ, and burnout zone.

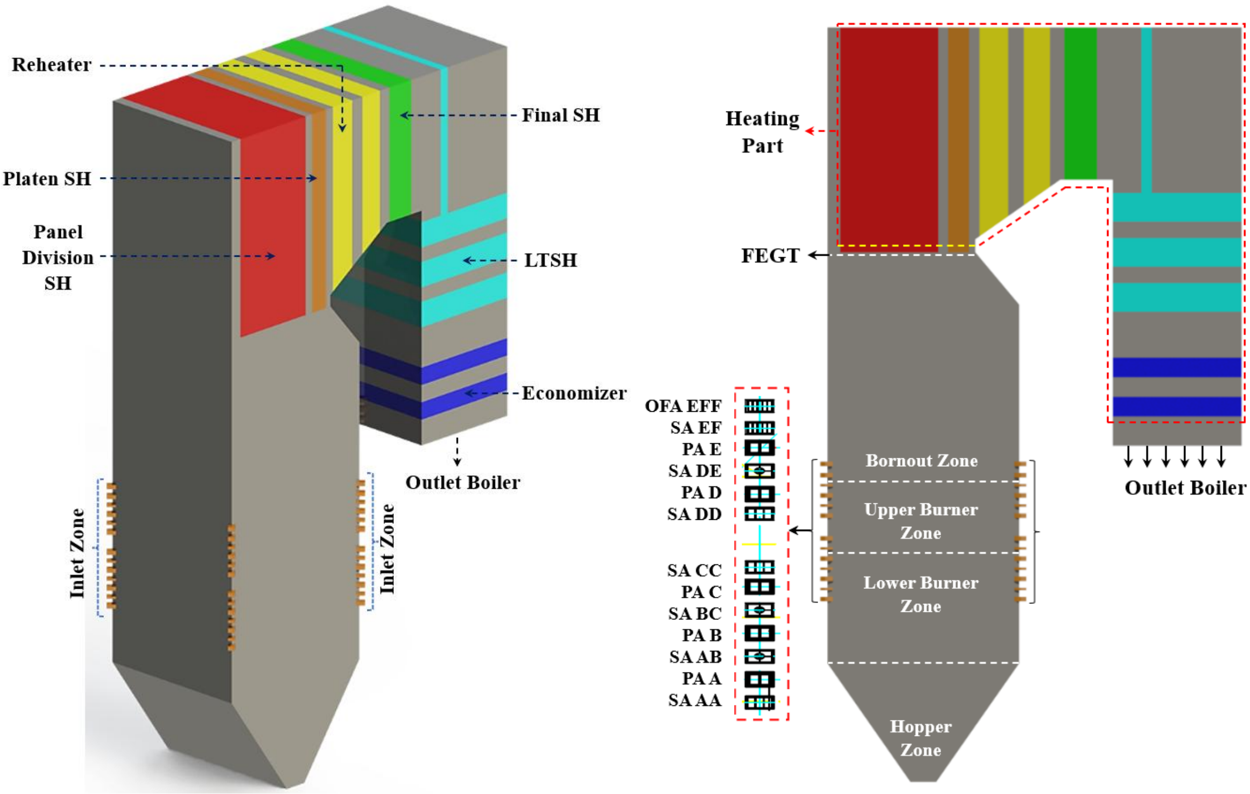

Figure 1. Schematic geometry of the PC boiler

Table 1. Material properties of LRC and EFB

	Ultimate Analysis (wt %)					Proximate Analysis (wt %)				
	(C)	(H)	(N)	(O)	(S)	(TM)	(VM)	(FC)	(AC)	Calorific value (kcal/kg)
LRC	71.07	4.99	1.00	22.75	0.18	31.43	33.76	32.31	2.50	4452
EFB	45.36	5.59	0.62	40.34	0.08	4.81	73.57	17.42	3.29	4174

Following the combustion process, flue gas from the boiler's burnout zone proceeds to the FEGT system, where heating components absorb heat. These components are assumed to be a porous medium consisting of Division-SH plates, #Platen-SH, #Reheater, #Final-SH, #LTSH, and #Economizer. The remaining combustion gases exit through the outlet of the PC boiler.

2.2 Numerical set-up

The CFD numerical-based simulation conducted in this study employs the Reynolds-Averaged Navier-Stokes (RANS) equations [26] using the ANSYS FLUENT application (version R2 2023) [27]. In the furnace of the PC boiler, the primary fuel combustion process involves LRC with the additional substitution of EFB. The reaction is modeled using the Finite-rate/Eddy-dissipation approach [34] within the species transport model (STM) [35, 36], and the tracking of the spent fuel particles is performed using the Eulerian-Lagrangian method [37] conforming to Rossin-Rammler distribution. The particle size varies, with a minimum diameter of 70 µm, a maximum diameter of 200 µm, and a mean diameter of 134 µm in the discrete phase model [38, 39]. To model the radiant heat occurring around the PC boiler furnace, the discrete ordinate (DO) model is employed [25, 40] with an applied scattering coefficient and emissivity of 0.6. The domain-based weighted sum of gray gases model (WSGGM) is selected for combustion gas absorption [41, 42]. The set-up is modeled using the SIMPLE Viscous Standard K-ε Wall Fn method [43, 44] details of the numerical equations in Table 2. The primary equations used in the simulation of coal combustion (LRC) and co-firing mixtures (EFB) in PC boilers include mass, momentum, energy, and species conservation [45, 46], which are presented in equations 1-4 as follows:

Mass conservation:

$$\frac{\partial}{\partial x_a}(\rho \mathcal{U}_a \pi r^2 = \sum_b S_b \tag{1}$$

Momentum conservation:

$$\frac{\partial}{\partial x_a}(\rho \mathcal{U}_a \mathcal{U}_b) + \frac{\partial P}{\partial x_b} = \frac{\partial}{\partial x_a}\left[\mu\left\{\frac{\partial u_b}{\partial x_a} + \frac{\partial u_a}{\partial x_b} - \frac{2}{3}\delta_{ab}\frac{\partial u_a}{\partial x_a}\right\}\right] + \frac{\partial}{\partial x_a}(-\rho \mu_b \mu_a) - F_p \tag{2}$$

Energy conservation:

$$\frac{\partial}{\partial x_a}(\mathcal{U}_a[\rho E + P])\frac{\partial}{\partial x_b}\left[\lambda_{eff}\frac{\partial T}{\partial x_b}\right] + S_h \tag{3}$$

Species conservation :

$$\frac{\partial}{\partial x_a}(\rho \mathcal{U}_b Y_c = -\frac{\partial}{\partial x_b}(\vec{J}_c) + \dot{\omega}_c + S_c \tag{4}$$

The fuel and gas phases of the particle reactions are simplified into two stages. The combustion reactions for each LRC char and EFB char can be expressed as follows:

$$\text{LRC char (C)} + 0.5\ O_2 \rightarrow CO \quad (5)$$

$$\text{EFB char (C)} + 0.5\ O_2 \rightarrow CO \quad (6)$$

Combustion reactions for LRC and EFB fuel in the PC boiler used in this study are as follows:

$$\text{LRC}: C_{1.11} H_{2.93} O_{0.84} N_{0.0042} S_{0.0033} + 0.87\ O2 \rightarrow 1.11\ CO + 1.46\ H_2O + 0.0021\ N_2 + 0.0033\ SO_2 \quad (7)$$

$$\text{EFB}: C_{0.93} H_{2.29} O_{1.02} N_{0.0017} S_{0.0010} + 1.00\ O_2 \rightarrow 0.93\ CO_2 + 1.14\ H_2O + 0.0008\ N_2 + 0.0010\ SO_2 \quad (8)$$

$$CO + 0.5\ O_2 \rightarrow CO_2 \quad (9)$$

2.3 Meshing process

In this study, the mesh system for the computational domain of the PC boiler is created using ANSYS Fluent meshing and modeled with real-scale dimensions [47]. The computational domain of the PC boiler mesh is illustrated in Figure 2. Given the complexity of the PC boiler's construction, it is essential to simplify the model by dividing it into several components. These components are integrated using the shared topology feature to optimize the mesh results. The Multizone All Body set-up employs the mapped/swept type Hexahedral method with a quadratic element order [48].

For the inlet burner, the mesh edge sizing method was applied by specifying the number of divisions along the connecting lines of each burner group on all four sides of the PC boiler. A detailed mesh configuration for the inlet burner section is illustrated in Figure 2. Using too few elements in a mesh domain leads to less accurate calculations, whereas an excessive number of elements prolongs the time required for numerical computations [49].

To address this issue, three mesh models were considered: Meshing #X, Meshing #Y, and Meshing #Z, each designed to manage the complexity of the PC boiler domain effectively. The mesh demonstrating the best performance was selected based on orthogonal quality (minimum 0.63, average 0.98) and skewness (minimum 1.358E-010, maximum 0.55) [25, 50].

The result of the grid independence test, which is essential for determining the meshing model, must be validated for accuracy. The benchmark for this validation is the temperature value recorded at the furnace exit gas temperature of the PC boiler. Actual conditions indicate that the design temperature of the PC boiler in the FEGT area is 1258.2 K. In simulations, the temperature recorded for Meshing #X is 1317.62 K, Meshing #Y is 1305.80 K, and Meshing #Z is 1308.17 K. Boundary conditions for the simulation of all cases can be seen in Table 3. Therefore, the #Y meshing model has been selected for the entire numerical simulation of this study, as detailed in Table 4.

Table 2. Equations for simulation in steady state condition for EFB Co-firing [51, 52]

Application type	Formulas	Models
Gas-Solid Model	$\frac{d\vec{u}_p}{dt} = F_D(\vec{u} - \vec{u}_p) + \frac{\vec{g}(\rho_p - \rho)}{p_\rho}$	RANS
Viscous	$\frac{\partial}{\partial t}(\rho\varepsilon) + \frac{\partial}{\partial x_i}(p\varepsilon u_i) = \frac{\partial}{\partial x_j}\left[\left(u + \frac{u_t}{u_\varepsilon}\right)\frac{\partial_\varepsilon}{\partial x_j}\right] + C_{1\varepsilon}\frac{\varepsilon}{k}C_k - C_{2\varepsilon}\frac{\varepsilon^2}{k}$	K-epsilon Standard
Solid	$\frac{\partial}{\partial x}(\rho u_i u_\varphi) = \frac{\partial}{\partial x_i}\left(\Gamma_\varphi \frac{\partial_\varphi}{\partial x_i}\right) + S_\varphi$	Discrete Phase
Turbulent dispersion	$\mu_t = \rho C_\mu \frac{k^2}{\varepsilon}$	Discrete random walk
Absorption coefficient	$\varepsilon = \sum_{i=0}^{I}\sum_{j=1}^{J} b_{\varepsilon,i,j} T^{j-1}(1 - e^{-k_i ps}$	WSGGM
Coal devolatilization	$\frac{m_v(t)}{(1 - f_{w,0})m_{p,0} - m_a} = \int_0^t (a_1\Re_1 + a_2\Re_2)\exp\left(\int_0^t (\Re_1 + \Re_2)dt\right)dt$	Two Competing rates
Radiation	$\frac{dI(t,u)}{ds} + (a + \sigma_s)I(t,u) = an^2\frac{\sigma T^4}{\pi} + \frac{\sigma_s}{4\pi}\int_0^{4\pi} I(t,u')\phi(u \cdot u')d\Omega$	Discrete Ordinate

Table 3. Boundary condition for injection at different burner zones in the PC boiler

Item	Operating PC Boiler	Simulation Cases					
Case	100% LRC	Case 1	Case 2	Case 3	Case 4	Case 5	Case 6
Combustion type	Pure Coal	Co-firing					
EFB bleeding ratio (%, thermal basis)	0	5	5	15	15	25	25
Fuel mills in service (burn zone)	ABCD	A	D	A	D	A	D
Coal feed rates (kg/s)	42.16	39.91	39.91	35.42	35.42	30.92	30.92
Biomass feed rates (kg/s)	-	2.25	2.25	6.74	6.74	11.24	11.24
PA a flow rate (kg/s)	97.62						
SA a flow rate (kg/s)	189.9						
CCOFA a flow rate (kg/s)	44.35						
Temperature of PA (°C)	56.8						
Temperature of SA and CCOFA (°C)	325.9						

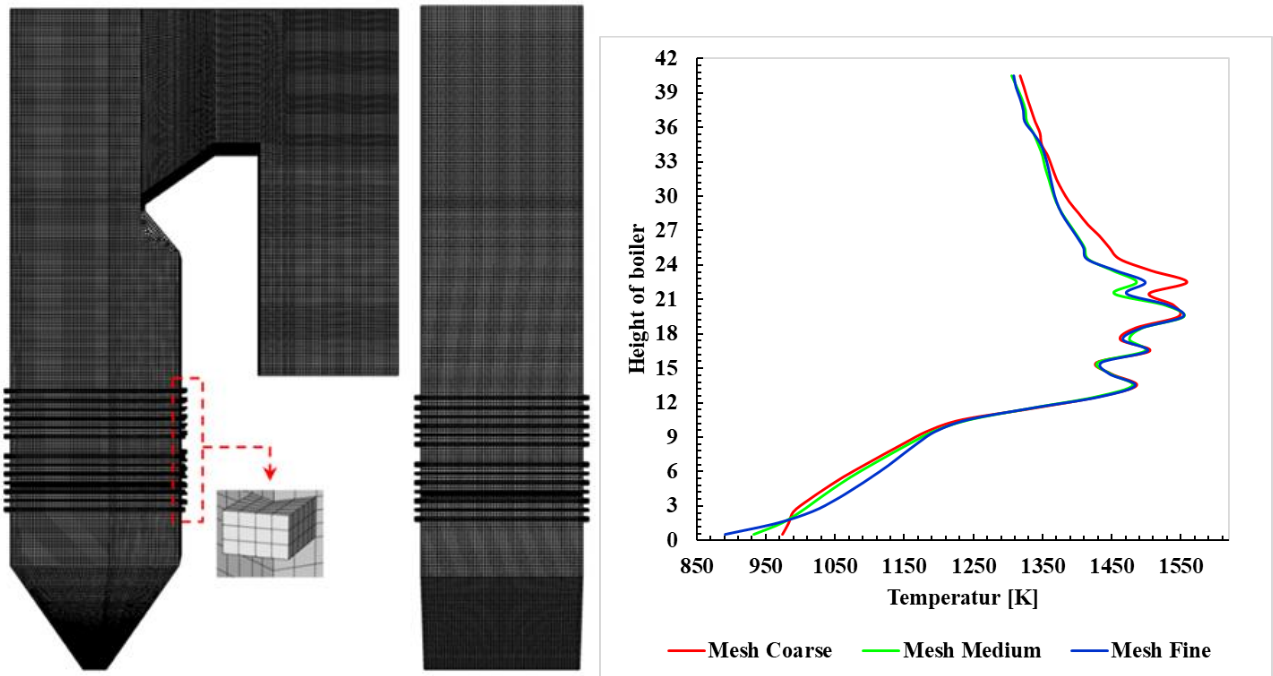

(a) PC boiler meshing (b) Grid independence test PC boiler

Figure 2. PC boiler structure meshing result

Table 4. Mesh data for grid independence test

Meshing Model	Elements	Nodes	Deviations Error
Meshing #X	1,370,792	1,316,252	4.72%
Meshing #Y	1,634,732	1,696,408	3.78%
Meshing #Z	1,876,480	1,944,507	4.00%

3. RESULT

3.1 Temperature distribution

LRC combustion is characterized by a longer residence time required to achieve stable conditions due to its high water content and low calorific value. When co-firing with solid waste from palm oil, specifically in the form of empty fruit bunches (EFB), notable differences in combustion characteristics arise between LRC and EFB. Temperature is a key parameter for analyzing the combustion state of the entire PC boiler. When EFB is injected as a mixture in the combustion chamber, temperature variations can be observed across different burner zones (Burner A and Burner D). The cross-section at the midpoint of the boiler, along with cuts at each burner elevation, is selected to represent the temperature contour for the 100% LRC simulation case, as illustrated in Figure 3. Figure 4 depicts the temperature distribution for the EFB co-firing injection cases 1 through 6. The temperature contours indicate that co-firing coal with empty fruit bunches (EFB) at caloric contents of 5%, 15%, and 25%, using injections from different burners (A and D), results in temperature increases at each burner elevation compared to 100% LRC combustion. The average temperature increase from full coal combustion to various levels of co-firing for burners A and D is as shown in Table 5.

The temperature increases for each burner elevation are depicted in Figures 3 and 4. These figures demonstrate that EFB injection at burner D results in a significantly greater temperature increase compared to burner A at the same co-firing levels, particularly when contrasted with full coal combustion. This phenomenon can be attributed to the chemical properties of EFB. The high volatile matter (VM) content in EFB enhances the combustion rate and reactivity of the fuel. Additionally, the low total moisture (TM) and fixed carbon (FC) contents in EFB are favorable for minimizing energy loss, which contributes to an increase in temperature within the combustion chamber.

Table 5. Average levels temperature

For Burner A	For Burner D
Case 1: 9.74 K	Case 2: 54.82 K
Case 3: 24.83 K	Case 4: 72.30 K
Case 5: 34.10 K	Case 6: 85.36 K

Figure 5 illustrates the combustion characteristics based on the average temperature from the hopper zone to the exit furnace (FEGT) in the middle cross-section of the PC boiler. It is observed that the overall characteristics do not differ significantly between the 100% LRC and co-firing EFB cases 1-6. Fuel combustion primarily occurs in the center of the furnace, specifically in the LBZ at the inlet for burner A and in the UBZ at the inlet for burner D. The highest temperature is recorded near the UBZ in the main region, indicating that the fuel begins to ignite after being injected into the furnace from the burner inlet. The symmetrical tangent circles formed by the temperature distribution are characteristic of tangentially fired boiler combustion. The Hopper Zone (HZ), located below the LBZ, collects the residual ash particles at the conclusion of the fuel combustion process. Ideally, this area should maintain the lowest temperature. Under real conditions, some ash particles typically flow to the exit furnace along with the combustion flue gas. As the levels of EFB co-firing increase from 5% to 25%, the FEGT temperature gradually decreases from approximately 1300 K to below 1290 K. In each co-firing scenario, the temperature difference between burner A and burner D is minimal;

however, burner D generally exhibits slightly lower temperatures than burner A. For instance, at 5% EFB, burner D has a temperature of 1306.77 K, which is marginally higher than burner A's temperature of 1300.26 K. Conversely, at 15% and 25% EFB, burner D constantly exhibits slightly lower temperatures than burner A.

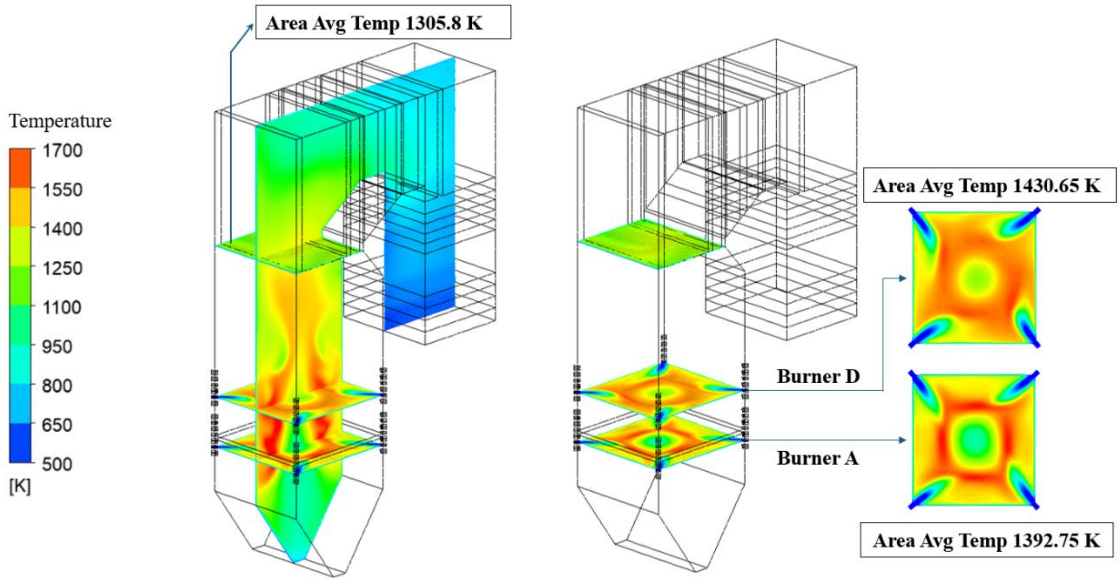

Figure 3. Temperature distribution of 100% LRC

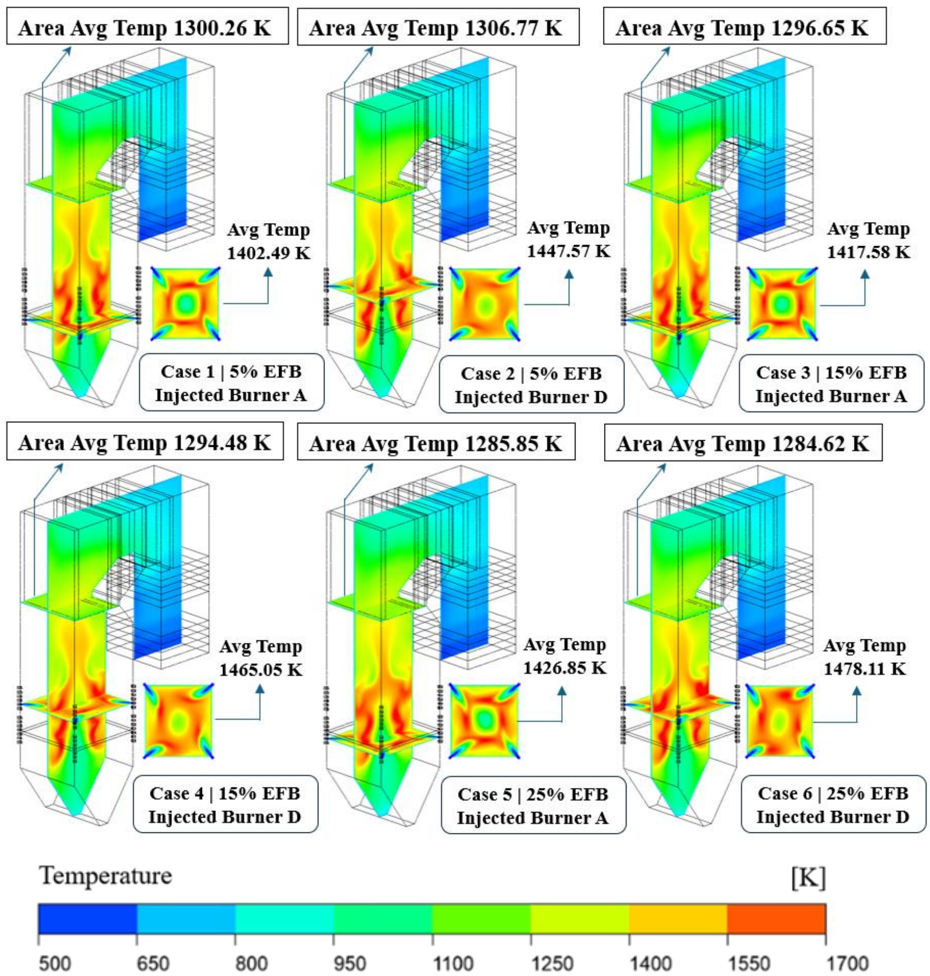

Figure 4. Temperature distribution of EFB co-firing Case 1-6

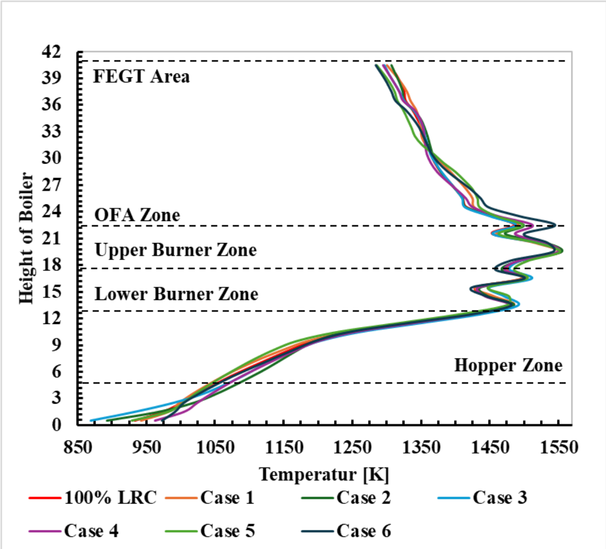

Figure 5. Temperature distribution curve

3.2 Distribution of mass fraction CO_2

Figures 6 and 7 show the distribution of Mass Friction of CO_2 in the PC Boiler, presented in 3-dimensional form and horizontal slices to display the contours at the injection points of burner A and burner D. The average CO_2 at the outlet of the 100% LRC PC Boiler is slightly higher (0.1962) compared to all co-firing scenarios (ranging from 0.1940 - 0.1959). The overall characteristics of the 100% LRC CO_2 distribution indicate higher concentrations in some regions of the boiler compared to the co-firing scenarios. In contrast, the EFB co-firing case exhibits a more uniform CO_2 distribution, albeit with a slightly lower average concentration. Notably, EFB injection in burner A tends to increase the average CO_2 compared to burner D. Case 5 (25% EFB in burner A) records the highest average CO_2 concentration in burner A (0.2034), surpassing the 100% LRC concentration in burner A (0.19099). Similarly, Case 6 (25% EFB in burner D) shows an average CO_2 concentration in burner D (0.1894) that is higher than that of 100% LRC in burner D (0.182917).

Figure 8 presents a comparison curve of the Mass Fraction distribution of CO_2 relative to the height of the PC boiler, spanning from the hopper zone section to the flue gas exit temperature (FEGT). In all instances of co-firing with empty fruit bunches (EFB) and 100% LRC, biomass such as EFB tends to produce less CO_2 compared to coal (LRC). Under the 100% LRC condition, the CO_2 concentration remains relatively stable at various heights within the boiler. In the EFB co-firing cases, from Case 1 to Case 6, all scenarios exhibit a similar trend, with CO_2 concentration beginning to decrease after reaching a height of approximately 25 m.

Case 5, in particular, exhibits the most significant decrease in CO_2 concentration after reaching a height of 25 m compared to other cases. The graph indicates that each co-firing scenario has a higher CO_2 concentration at lower altitudes than the 100% LRC case; however, the concentration decreases more sharply at higher altitudes. At the bottom of the boiler (approximately 0.5 m to 20.5 m height), the CO_2 mass fraction is high in PC boilers. This phenomenon occurs because the primary combustion occurs at the bottom of the boiler. Since most of the coal combusts burn in this area, the CO_2 concentration is higher due to the intensive combustion process. Although the hopper zone is not directly involved in the main combustion process, it can still contain a relatively high CO_2 content. While the primary combustion occurs above the hopper zone, the combustion gases, including CO_2, can flow downward and accumulate in this area before being discharged through the exhaust system.

The use of EFB as an auxiliary fuel tends to decrease the CO_2 mass fraction at the boiler outlet compared to the use of 100% LRC as can be seen in Figure 9. Cases 5 and 6 demonstrate the most significant reduction in CO_2 mass fraction (~0.1940), suggesting that the injection of 25% EFB in burners A and D effectively reduces CO_2 emissions. In all co-firing scenarios, the CO_2 mass fraction at the boiler outlet is lower than that of 100% LRC, indicating that the addition of EFB as a fuel improves combustion efficiency or leads to cleaner combustion. Cases 1 and 2 (5% EFB) exhibit a smaller reduction than Cases 3 and 4 (15% EFB) and Cases 5 and 6 (25% EFB). This trend suggests that increasing the proportion of EFB is more effective in reducing the CO_2 mass fraction. Furthermore, Cases 1 and 3 indicate that EFB injection in burner A results in a more significant reduction in CO_2 mass fraction compared to burner D in Cases 2 and 4, given the same EFB proportion. However, at higher EFB proportions (25%), the difference between burners A and D becomes negligible, as Cases 5 and 6 exhibit almost identical CO_2 mass fractions.

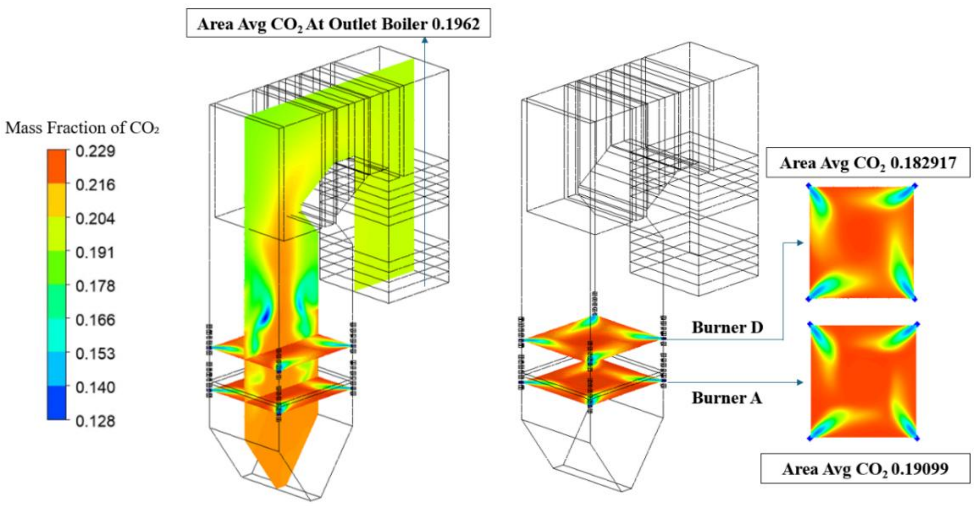

Figure 6. CO_2 distribution of the 100% LRC

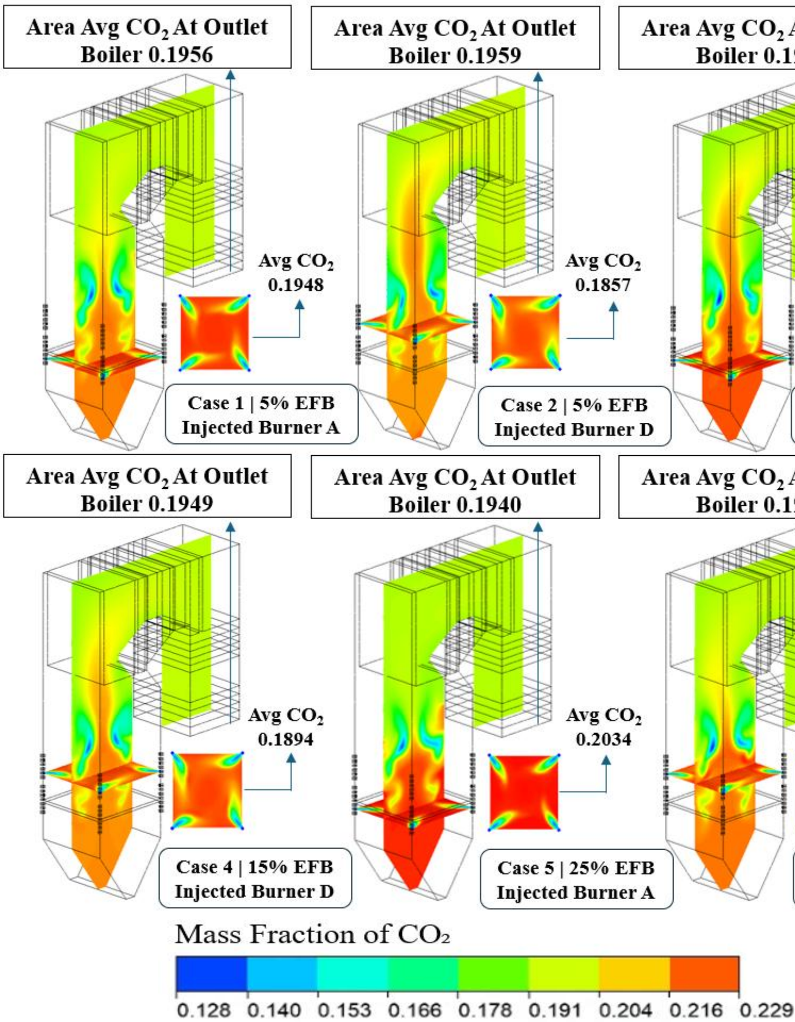

Figure 7. CO_2 distribution of co-firing EFB Case 1-6

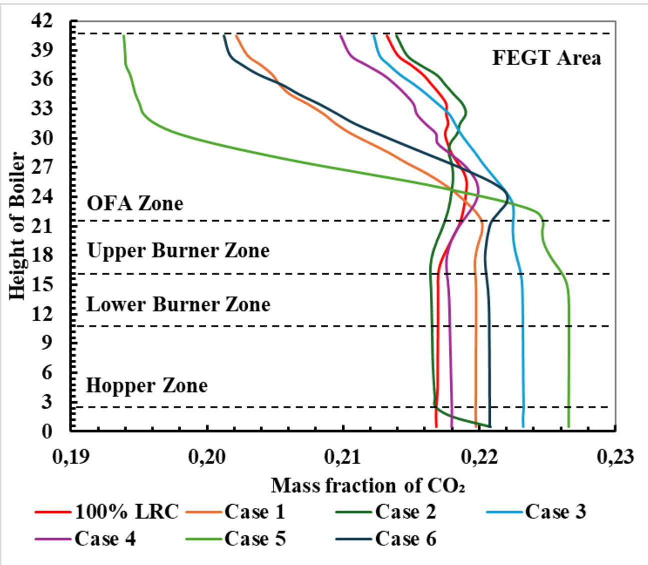

Figure 8. CO_2 distribution curve

3.3 Distribution of mass fraction NOx

Figure 10 and Figure 11 illustrate the distribution of NOx concentration. The increase in NOx concentration values indicates a rising trend in the main Furnace area, specifically in the UBZ, during Co-firing under 5% ammonia conditions at each burner injection point A-D. The significant levels of fuel NOx and thermal NOx can be attributed to the high combustion intensity, which leads to an increased temperature. Subsequently, further reduction occurs in the UPC and OFA sections, resulting in a NOx concentration as it reacts to form Nitrogen.

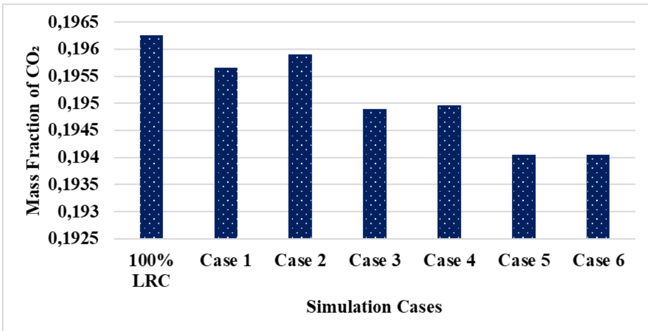

Figure 9. Graph of mass fraction of CO_2 at boiler outlet

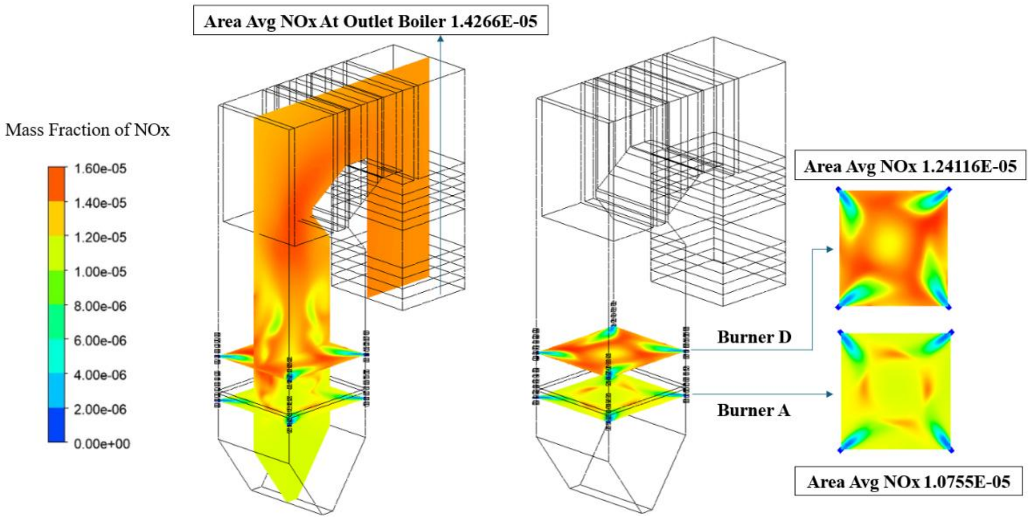

Figure 10. NOx distribution of 100% LRC

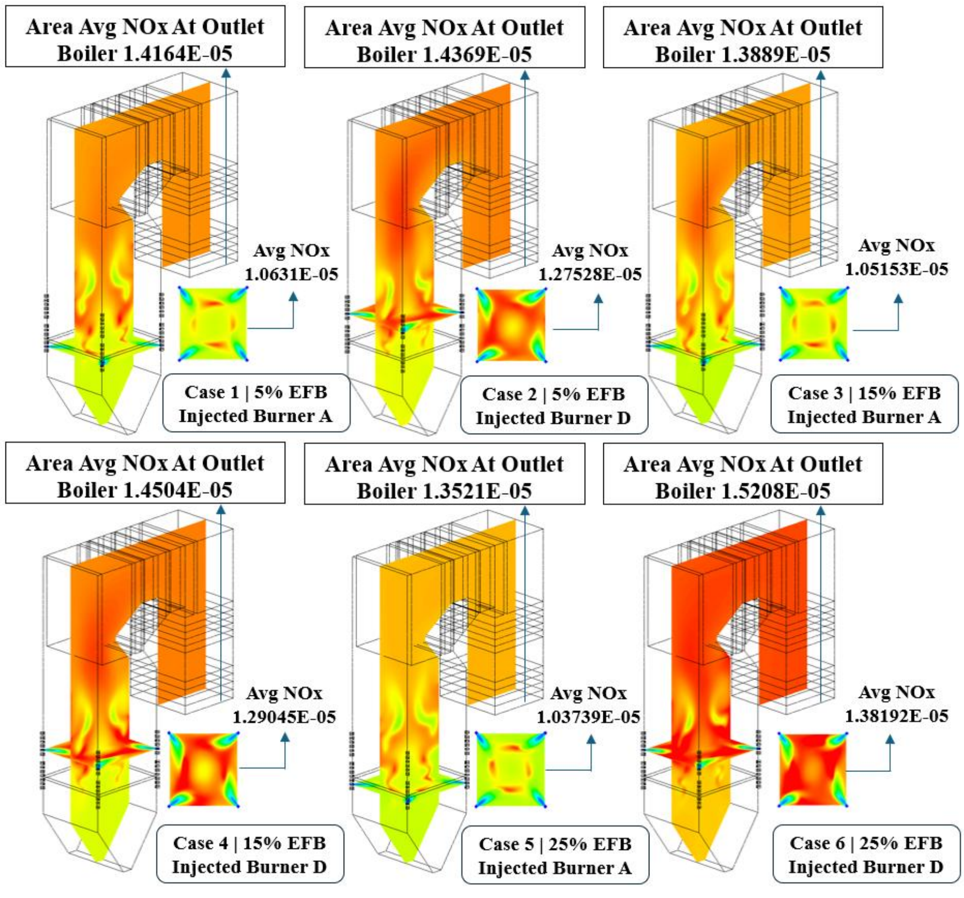

Figure 11. NOx distribution of EFB co-firing Case 1-6

Figure 12 illustrates the distribution of NOx mass fraction at various boiler heights for the 100% LRC case and six EFB (Empty Fruit Bunches) co-firing scenarios. The graphical analysis indicates that co-firing with EFB generally leads to a reduction in NOx emissions compared to the use of full coal (100% LRC). In the case of 100% LRC, the NOx mass fraction consistently increases with boiler height, with significant increases observed in the Over Fire Air (OFA) and Furnace Exit Gas Temperature (FEGT) zones. This trend suggests that full coal combustion results in high NOx emissions, particularly at the top sections of the boiler: in the EFB co-firing scenarios, each case (case 1 to case 6) exhibits variations in the NOx mass fraction distribution. However, in general, all EFB co-firing scenarios demonstrate a reduction in NOx emissions compared to 100% LRC. Notable decreases were observed in the OFA and FEGT zones, demonstrating the effectiveness of EFB co-firing in mitigating NOx emissions at greater heights within the boiler.

In Figure 13, the distribution of SO_2 mass fraction varies between full coal combustion and various scenarios of EFB co-firing, indicating a significant effect of mixed fuel use on SO_2 emissions in the boiler. The implementation of EFB co-firing generally results in a reduction in SO_2 mass fraction across different boiler zones compared to full coal combustion. This reduction can be attributed to the distinct combustion characteristics of EFB, which include lower sulfur content and varying reactivity. Specifically, these findings highlight the potential of reducing SO_2 emissions through the application of EFB co-firing technology, representing a crucial step toward mitigating the environmental impact of fossil fuel combustion. However, the variation in SO_2 distribution among the the co-firing cases suggests that further optimization of the mixing ratio and operating conditions is necessary to achieve maximum emission reduction efficiency.

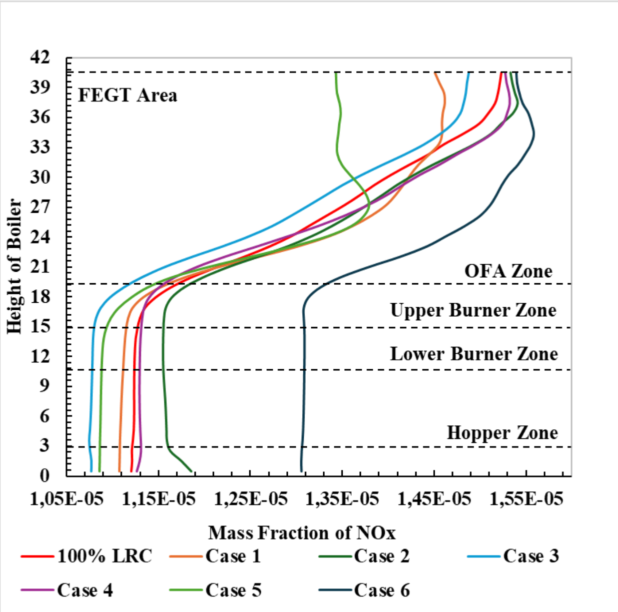

Figure 12. NOx mass fraction distribution curve

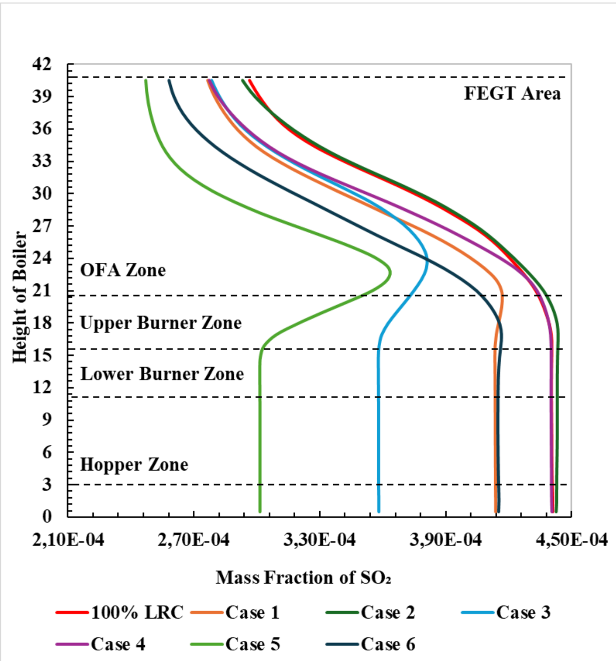

Figure 13. SO_2 mass fraction distribution curve

This study examines the effect of using different burners on NOx and SO_2 emissions under 100% LRC conditions, as well as in various cases of EFB co-firing and their impact at the boiler outlet. According to the simulation results presented in Figure 12, there is a significant difference in NOx and SO_2 emissions between the burners located at the bottom of the boiler (Burner A) and those positioned at the top of the boiler (Burner D).

In the 100% LRC condition, NOx and SO_2 emissions reached their highest levels compared to all EFB co-firing cases. This finding indicates that the use of 100% LRC leads to less efficient combustion, resulting in high emissions. Significant reductions in NOx and SO_2 emissions were observed in the EFB co-firing cases, especially in the scenario using Burner A. Burner A (LBZ), used in Cases 1, 3, and 5, demonstrated a more substantial reduction in emissions compared to Burner D (UBZ), which was used in Cases 2, 4, and 6. In Cases 1, 3, and 5, NOx and SO_2 emissions were lower than those in Cases 2, 4, and 6. This difference may be attributed to improved heat distribution and airflow at the bottom of the boiler, facilitating more efficient and uniform combustion. The increase in emissions observed in Case 6, where Burner D is used, suggests that combustion at the top of the boiler may be less efficient. Suboptimal heat distribution and uneven airflow at the top of the boiler can lead to incomplete combustion, resulting in increased NOx and SO_2 emissions. The impact of this difference is also evident in the emissions at the boiler outlet in Figure 14. When using Burner A, the reduction in NOx and SO_2 emissions at the boiler outlet is more pronounced than with Burner D. This finding indicates that the position of the burner not only influences the combustion process in the boiler but also affects the quality of emissions produced at the boiler outlet. Lower emissions at the boiler outlet indicate comprehensive and efficient combustion, thereby decreasing the amount of pollutants released into the atmosphere. Overall, the findings of this study demonstrate that burner location significantly influences NOx and SO_2 emissions and the quality of emissions at the boiler outlet. The use of Burner A, positioned at the bottom of the boiler, tends to produce lower emissions compared to Burner D, which is located at the top. Therefore, optimizing burner location and other operational conditions is essential for reducing emissions in the combustion process.

Table 6 compares the key findings of this study with those of previous studies on EFB co-firing. Unlike the studies conducted by Jiang et al. [23] and Darmawan et al. [25], which focused on the effect of biomass type and ratio on combustion efficiency and flue gas emissions, this study introduces a new dimension by examining the impact of burner position on the performance of EFB and coal co-firing. Previous research has not explicitly assessed how the spatial distribution of fuels within the burner influences temperature distribution and emissions. In addition, research by Hariana et al. [20] indicated a tendency for slagging and fouling when co-firing EFB and FRD; however, it did not examine potential mitigation strategies through combustion design aspects.

In this study, the findings indicate that utilizing a lower burner position (Burner A) significantly reduces CO, NOx, and SO_2 emissions when the EFB ratio is set at 25%; this provides new insights, suggesting that adjusting fuel distribution within the burner can serve as an effective operational strategy for improving co-firing performance. Consequently, this study not only reinforces previous findings regarding the advantages of EFB co-firing but also makes a novel contribution by demonstrating that optimizing burner position can be a key factor in achieving lower emissions—an area that has not been extensively explored in previous literature.

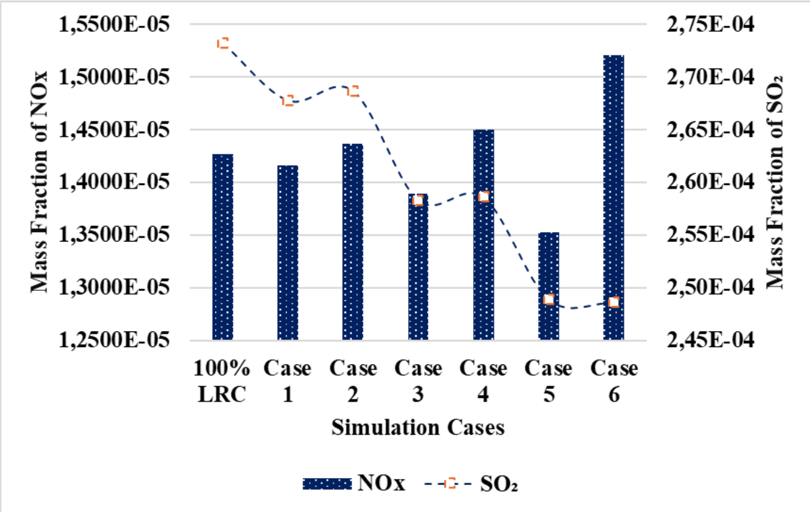

Figure 14. Comparison chart of NOx and SO_2 at boiler outlet for all cases

Table 6. Comparison of research results with previous studies

Study	Year	Method	Co-Firing Fuel	Parameter Studies	Key Finding
Darmawan et al. [25]	2017	CFD Simulation & Experimental Analysis	Hydrothermally-Treated Empty Fruit Bunch (HT-EFB) & Coal	Temperature, CO, CO_2, Combustion Efficiency	HT-EFB 10–25% was the optimal ratio for co-firing, increased combustion temperature, and reduced CO_2 emissions.
Jiang et al. [23]	2020	CFD Simulation & Experimental Analysis	Torrefied Empty Fruit Bunch (T-EFB) & Coal	Combustion, Heat Transfer, NOx & SO_2 Emissions	Co-firing T-EFB 40% began to reduce boiler efficiency; NOx & SO_2 significantly decreased with increased T-EFB substitution.
Hariana et al. [20]	2023	Experimental & CFD Simulation	Empty Fruit Bunch (EFB) & Palm Frond (FRD) with Coal	Slagging, Fouling, Temperature, Ash Behavior	Co-firing 25% biomass (EFB + FRD) increased slagging tendencies; SEM-EDX and XRD analysis showed that a 12.5% EFB + 12.5% FRD blend was better than using a single type of biomass.
Present Research	2025	CFD Simulation	Empty Fruit Bunch (EFB) & Low-Rank Coal	Burner Position, Temperature, CO_2, NOx, SO_2	The lower burner (Burner A) produced lower emissions; co-firing EFB 25% was most effective in reducing.

4. CONCLUSIONS

This study demonstrates that EFB co-firing in PC boilers can significantly enhance combustion performance and reduce emissions. Key findings indicate that top burner injection (D) achieves a maximum temperature increase (up to 85.36 K at 25% EFB), while the bottom burner configuration (A) results in substantial emission reductions of 12% for CO_2 and 18% for NOx at the same EFB percentage. The 25% EFB blend emerges as the optimal choice for balancing efficiency and environmental benefits. However, these conclusions are subject to the limitations inherent to CFD modeling, including the assumption of steady-state conditions, ideal particle size distribution, and simplified chemical kinetics. Future research should integrate experimental validation with industrial-scale testing to verify simulation results, particularly concerning ash deposition behavior and long-term burner performance. Additional research directions should focus on optimizing air-staging strategies and assessing the economic feasibility of large-scale EFB co-firing implementation. These advancements will facilitate the transition toward sustainable biomass utilization in coal-fired power plants.

REFERENCES

[1] Yang, S., Yang, D.Z., Shi, W., Deng, C.C., Chen, C.B., Feng, S.J. (2022). Global evaluation of carbon neutrality and peak carbon dioxide emissions: Current challenges and future outlook. Environmental Science and Pollution Research, 30(34): 81725-81744.7 https://doi.org/10.1007/s11356-022-19764-0

[2] Omotoso, A.B., Omotayo, A.O. (2023). The interplay between agriculture, greenhouse gases, and climate change in Sub-Saharan Africa. Regional Environmental Change, 24(1). https://doi.org/10.1007/s10113-023-02159-3

[3] Gani, A. (2021). Fossil fuel energy and environmental performance in an extended STIRPAT model. Journal of Cleaner Production, 297: 126526. https://doi.org/10.1016/j.jclepro.2021.126526

[4] Capellán-Pérez, I., Arto, I., Polanco-Martínez, J.M., González-Eguino, M., Neumann, M.B. (2016). Likelihood of climate change pathways under uncertainty on fossil fuel resource availability. Energy & Environmental Science, 9(8): 2482-2496. https://doi.org/10.1039/c6ee01008c

[5] Agbor, E., Zhang, X., Kumar, A. (2014). A review of biomass co-firing in North America. Renewable and Sustainable Energy Reviews, 40: 930-943. https://doi.org/10.1016/j.rser.2014.07.195

[6] De Laporte, A.V., Weersink, A.J., McKenney, D.W. (2016). Effects of supply chain structure and biomass prices on bioenergy feedstock supply. Applied Energy,

183: 1053-1064. https://doi.org/10.1016/j.apenergy.2016.09.049
[7] Mohd Idris, M.N., Hashim, H., Razak, N.H. (2018). Spatial optimisation of oil palm biomass co-firing for emissions reduction in coal-fired power plant. Journal of Cleaner Production, 172: 3428-3447. https://doi.org/10.1016/j.jclepro.2017.11.027
[8] Savolainen, K. (2003). Co-firing of biomass in coal-fired utility boilers. Applied Energy, 74(3-4): 369-381. https://doi.org/10.1016/s0306-2619(02)00193-9
[9] Steer, J., Marsh, R., Griffiths, A., Malmgren, A., Riley, G. (2013). Biomass co-firing trials on a down-fired utility boiler. Energy Conversion and Management, 66: 285-294. https://doi.org/10.1016/j.enconman.2012.10.010
[10] Zahraee, S.M., Mokhtar, A.A., Tolooie, A., Mohd Asri, N.A. (2019). Performance evaluation of EFB biomass supply chain for electricity power generation based on computer simulation: Malaysia case study. Advances in Material Sciences and Engineering, 363-375. https://doi.org/10.1007/978-981-13-8297-0_39
[11] Tarigan, S.D., Sunarti, Widyaliza, S. (2015). Expansion of oil palm plantations and forest cover changes in Bungo and Merangin Districts, Jambi Province, Indonesia. Procedia Environmental Sciences, 24: 199-205. https://doi.org/10.1016/j.proenv.2015.03.026
[12] Badan Pusat Statistik - BPS, Indonesian Palm Oil Statistics 2022, 2020. https://www.bps.go.id/en/publication/2023/11/30/160f211bfc4f91e1b77974e1/indonesian-oil-palm-statistics-2022.html, accessed on Feb. 17, 2025.
[13] Roni, M.S., Chowdhury, S., Mamun, S., Marufuzzaman, M., Lein, W., Johnson, S. (2017). Biomass co-firing technology with policies, challenges, and opportunities: A global review. Renewable and Sustainable Energy Reviews, 78: 1089-1101. https://doi.org/10.1016/j.rser.2017.05.023
[14] Xu, J.P., Huang, Q., Lv, C.W., Feng, Q., Wang, F.J. (2018). Carbon emissions reductions oriented dynamic equilibrium strategy using biomass-coal co-firing. Energy Policy, 123: 184-197. https://doi.org/10.1016/j.enpol.2018.08.043
[15] Sugiyono, A., Febijanto, I., Hilmawan, E., Adiarso. (2022). Potential of biomass and coal co-firing power plants in Indonesia: A PESTEL analysis. IOP Conference Series: Earth and Environmental Science, 963(1): 012007. https://doi.org/10.1088/1755-1315/963/1/012007
[16] Aziz, M., Prawisudha, P., Prabowo, B., Budiman, B.A. (2015). Integration of energy-efficient empty fruit bunch drying with gasification/combined cycle systems. Applied Energy, 139: 188-195. https://doi.org/10.1016/j.apenergy.2014.11.038
[17] Yasin, C.M., Yunianto, B., Sugiarti, S., Hudaya, G.K. (2021). Implementation of Indonesia coal downstream policy in the trend of fossil energy transition. IOP Conference Series: Earth and Environmental Science, 882(1): 012083. https://doi.org/10.1088/1755-1315/882/1/012083
[18] Abdulrazik, A., Elsholkami, M., Elkamel, A., Simon, L. (2017). Multi-products productions from Malaysian oil palm empty fruit bunch (EFB): Analyzing economic potentials from the optimal biomass supply chain. Journal of Cleaner Production, 168: 131-148. https://doi.org/10.1016/j.jclepro.2017.08.088
[19] Miedema, J.H., Benders, R.M.J., Moll, H.C., Pierie, F. (2017). Renew, reduce or become more efficient? The climate contribution of biomass co-combustion in a coal-fired power plant. Applied Energy, 187: 873-885. https://doi.org/10.1016/j.apenergy.2016.11.033
[20] Hariana, Prabowo, Hilmawan, E., Milky Kuswa, F., Darmawan, A., Aziz, M. (2023). A comprehensive evaluation of co-firing biomass with coal and slagging-fouling tendency in pulverized coal-fired boilers. Ain Shams Engineering Journal, 14(7): 102001. https://doi.org/10.1016/j.asej.2022.102001
[21] Taha, T.J., Stam, A.F., Stam, K., Brem, G. (2013). CFD modeling of ash deposition for co-combustion of MBM with coal in a tangentially fired utility boiler. Fuel Processing Technology, 114: 126-134. https://doi.org/10.1016/j.fuproc.2013.03.042
[22] Aziz, M., Budianto, D., Oda, T. (2016). Computational fluid dynamic analysis of co-firing of palm kernel shell and coal. Energies, 9(3): 137. https://doi.org/10.3390/en9030137
[23] Jiang, Y., Park, K.H., Jeon, C.H. (2020). Feasibility study of co-firing of torrefied empty fruit bunch and coal through boiler simulation. Energies, 13(12): 3051. https://doi.org/10.3390/en13123051
[24] Li, J., Brzdekiewicz, A., Yang, W., Blasiak, W. (2012). Co-firing based on biomass torrefaction in a pulverized coal boiler with aim of 100% fuel switching. Applied Energy, 99: 344-354. https://doi.org/10.1016/j.apenergy.2012.05.046
[25] Darmawan, A., Budianto, D., Aziz, M., Tokimatsu, K. (2017). Hydrothermally-treated empty fruit bunch co-firing in coal power plants: A techno-economic assessment. Energy Procedia, 105: 297-302. https://doi.org/10.1016/j.egypro.2017.03.317
[26] Ghenai, C., Janajreh, I. (2010). CFD analysis of the effects of co-firing biomass with coal. Energy Conversion and Management, 51(8): 1694-1701. https://doi.org/10.1016/j.enconman.2009.11.045
[27] Rahman, M.N. (2022). Optimisation of solid fuel in-furnace blending for an opposed-firing utility boiler: A numerical analysis. CFD Letters, 14(9): 89-107. https://doi.org/10.37934/cfdl.14.9.89107
[28] Anissa Rizki, G., Zulmasyhur. (2024). Strategic planning in achieving net zero emissions: Case of biomass co-firing technology. Journal of Governance Innovation, 6(1): 78-91. https://doi.org/10.36636/jogiv.v6i1.3529
[29] Ministry of Environment and Forestry, Republic of Indonesia, Peraturan Menteri Lingkungan Hidup Dan Kehutanan Republik Indonesia Nomor 15 Tahun 2019 Tentang Baku Mutu Emisi Pembangkit Listrik Tenaga Termal, 2019, pp. 1-56. https://peraturan.bpk.go.id/Details/286526/permen-lhk-no-15-tahun-2019.
[30] European Union. (2015). Directive (EU) 2015/2193 on the limitation of emissions from medium combustion plants.
[31] National Renewable Energy Laboratory (NREL). (2021). Biomass Co-firing Policies in Asia: A Comparative Study. https://www.nrel.gov/docs/fy24osti/88998.pdf, accessed on Apr. 1, 2025.
[32] Ihsan, S., Prabowo, Widodo, W.A., Saputra, I.N.A.A., Hariana. (2024). Utilization of palm frond waste as fuel for co-firing coal and biomass in a tangentially pulverized coal boiler using computational fluid dynamic

analysis. Biomass, 4(4): 1142-1163. https://doi.org/10.3390/biomass4040063
[33] Agus Adi Saputra, I.N., Prabowo, Setiyawan, A., Bagus Wijaya Kusuma, I.G., Ihsan, S., Darmawan, A. (2024). Numerical simulation co-firing Of EFB and LRC injected at different burner levels in tangential combustion-type pulverized boilers. In 2024 10th International Conference on Smart Computing and Communication (ICSCC), Bali, Indonesia, pp. 328-332. https://doi.org/10.1109/icscc62041.2024.10690373
[34] Sun, Z.P., Huang, Y., Luan, Z.Y., Gao, S.J., You, Y.C. (2023). Three-dimensional simulation of a rotating detonation engine in ammonia/hydrogen mixtures and oxygen-enriched air. International Journal of Hydrogen Energy, 48(12): 4891-4905. https://doi.org/10.1016/j.ijhydene.2022.11.029
[35] Sandrin, S., Mazzei, L., Da Soghe, R., Fontaneto, F. (2024). Computational fluid dynamics prediction of external thermal loads on film-cooled gas turbine vanes: A validation of reynolds-averaged navier–stokes transition models and scale-resolving simulations for the VKI LS-94 test case. Fluids, 9(4): 91. https://doi.org/10.3390/fluids9040091
[36] Laubscher, R., Rousseau, P. (2019). Numerical investigation into the effect of burner swirl direction on furnace and superheater heat absorption for a 620 MWe opposing wall-fired pulverized coal boiler. International Journal of Heat and Mass Transfer, 137: 506-522. https://doi.org/10.1016/j.ijheatmasstransfer.2019.03.150
[37] Kim, G.M., Lisandy, K.Y., Lee, B.H., Jeon, C.H. (2024). Enhancement of reaction rate prediction of biomass: A focus on experimental and numerical simulation approaches. Journal of the Energy Institute, 113: 101504. https://doi.org/10.1016/j.joei.2023.101504
[38] Niemelä, N.P., Nowak Delgado, R., de Riese, T., Tolvanen, H., Fendt, S., Spliethoff, H., Joronen, T. (2021). Fuel-specific devolatilization parameters for detailed comparison of pulverized biomass fuels. Fuel, 286: 119309. https://doi.org/10.1016/j.fuel.2020.119309
[39] Liu, T., Wang, Y.G., Zou, L., Bai, Y.Y., Shen, T., Wei, Y.W., Li, F.X., Zhao, Q.X. (2024). Numerical investigation of stable combustion at ultra-low load for a 350 MW wall tangentially fired pulverized-coal boiler: Effect of burner adjustments and methane co-firing. Applied Thermal Engineering, 246: 122980. https://doi.org/10.1016/j.applthermaleng.2024.122980
[40] Wei, D.N., Zhang, Z.C., Wu, L.N., Wang, T., Sun, B.M. (2023). Ammonia blend ratio impact on combustion characteristics and NOx emissions during co-firing with sludge and coal in a utility boiler. Energy, 283: 129220. https://doi.org/10.1016/j.energy.2023.129220
[41] Yang, X.L., Xi, T., Qin, Y.B., Zhang, H., & Wang, Y.W. (2024). Computational fluid dynamics–Discrete phase method simulations in process engineering: A review of recent progress. Applied Sciences, 14(9): 3856. https://doi.org/10.3390/app14093856
[42] Liu, M.Y., Chen, S., Zhu, H.W., Zhou, Z.J., Xu, J.Y. (2023). Numerical investigation of ammonia/coal co-combustion in a low NOx swirl burner. Energy, 282: 128358. https://doi.org/10.1016/j.energy.2023.128358
[43] Zhao, S.N., Fang, Q.Y., Yin, C.G., Wei, T.S., Wang, H.J., Zhang, C., Chen, G. (2017). New fuel air control strategy for reducing NOx emissions from corner-fired utility boilers at medium-low loads. Energy and Fuels, 31(7): 6689-6699. https://doi.org/10.1021/acs.energyfuels.7b00337
[44] Tabet, F., Gökalp, I. (2015). Review on CFD based models for co-firing coal and biomass. Renewable and Sustainable Energy Reviews, 51: 1101-1114. https://doi.org/10.1016/j.rser.2015.07.045
[45] Zheng, H.Q., Zhu, B.Z., Wang, Y.N., Sun, Y.L. (2023). Numerical study on the effects of co-firing ratio and stoichiometric ratio on biomass/ammonia co-firing. Journal of the Energy Institute, 111: 101364. https://doi.org/10.1016/j.joei.2023.101364
[46] Cardoso, J.S., Silva, V., Chavando, J.A.M., Eusébio, D., Hall, M.J. (2022). Numerical modelling of the coal phase-out through ammonia and biomass co-firing in a pilot-scale fluidized bed reactor. Fuel Communications, 10: 100055. https://doi.org/10.1016/j.jfueco.2022.100055
[47] Sousa Cardoso, J., Silva, V., Eusébio, D., Tarelho, L.A.C., Hall, M.J., Grinberg Dana, A. (2022). Numerical modelling of ammonia-coal co-firing in a pilot-scale fluidized bed reactor: Influence of ammonia addition for emissions control. Energy Conversion and Management, 254: 115226. https://doi.org/10.1016/j.enconman.2022.115226
[48] Rousseau, P., Laubscher, R. (2020). Analysis of the impact of coal quality on the heat transfer distribution in a high-ash pulverized coal boiler using co-simulation. Energy, 198: 117343. https://doi.org/10.1016/j.energy.2020.117343
[49] Yang, Y.N., Hori, T., Sawada, S., Akamatsu, F. (2024). Numerical investigation on the effects of air-staged strategy and ammonia co-firing ratios on NO emission characteristics using the Conjugate heat transfer method. Fuel, 368: 131591. https://doi.org/10.1016/j.fuel.2024.131591
[50] Yao, Z.P., Liu, J.Q., Qiu, Z.Z., Pan, W.G., Wu, Z.X. (2021). Numerical investigation of 700°C boiler flue gas thermal deviation based on orthogonal experiment. Fuel, 295: 120510. https://doi.org/10.1016/j.fuel.2021.120510
[51] Adi Saputra, I.N.A., Manurung, T.D., Yuliadi, A.E., Prabowo, Nugroho, G., Kusumadewi, T.V., Hariana, H., Chan, S.H. (2024). Numerical simulation of co-firing LRC and ammonia in Pangkalan Susu 3 & 4 coal-fired steam power plant (CFSPP) capacity 210 megawatts. Case Studies in Thermal Engineering, 63: 105230. https://doi.org/10.1016/j.csite.2024.105230
[52] Abdulwahab, M.R., Al-attab Al-attab, K.A., Idroas, M.Y. (2023). Numerical investigation and comparison between internal and external liquid biofuel pre-evaporation in micro gas turbine chamber. CFD Letters, 15(11): 181-200. https://doi.org/10.37934/cfdl.15.11.181200

NOMENCLATURE

CFD	computational fluid dynamic
CPO	crude palm oil
DO	discrate ordinate
DTF	drop tube furnance
EBT	renewable energy
EFB	empty fruit bunch
FC	fixed carbon
FEGT	furnance exit-gas temperature
LBZ	lower burner zone

LRC	low rank coal
MW	mega watts
UBZ	upper burner zone
HZ	hopper zone
OFA	over fire air
PA	primary air
PC	pulverized coal
RANS	reynolds-averaged-navier-stokes
SA	secondary air
TM	total moisture
VM	volatile metter

Equation symbol

$\vec{u}_p$	particle velocity
F_D	drag force
$\vec{u}$	fluid velocity
ρ_p	particle density
ρ	fluid density
$\vec{g}$	gravitational acceleration
ε	dissipation rate of turbulent kinetic energy
k	turbulent kinetic energy
u_t	turbulent viscosity
C_k	production of turbulent kinetic energy
C_1, C_2	model constants
u_i	velocity component
φ	scalar quantity (mass, momentum, etc.)
Γ_φ	diffusion coefficient
S_φ	source term
C_μ	empirical constant
$b_{\varepsilon,i,j}$	empirical coefficients
k_i	spectral absorption coefficient
ps	path length times partial pressure of gas
$m_v(t)$	mass of volatiles at time t
$f_{w,0}$	initial moisture fraction
$m_{p,0}$	initial particle mass
m_a	ash mass
a_1, a_2	pre-exponential factors for the two reactions
$\Re_1, \Re_2$	reaction rates
$I(t, u)$	radiative intensity
a	absorption coefficient
σ_s	scattering coefficient
T	temperature
σ	stefan-boltzmann constant
$\phi(u \cdot u')$	scattering phase function
S_m	source term related to mass (kg/(m³·s))
P	pressure
T	stress tensor (Pa)
F	external force vector (N/m³)